Conductivity and Time–Temperature Correspondence in Polar Viscoelastic Liquids

ARTICLE *in* MACROMOLECULES · APRIL 2013

Impact Factor: 5.8 · DOI: 10.1021/ma400224x

Macromolecules

Article

pubs.acs.org/Macromolecules

Conductivity and Time−Temperature Correspondence in Polar Viscoelastic Liquids

M. Carsí, M. J. Sanchis,* P. Ortiz-Serna, B. Redondo-Foj, and R. Díaz-Calleja

Energy Technological Institute (ITE), Universitat Politècnica de València, Camino de Vera s/n 46022, Valencia, Spain

E. Riande

Institute of Polymer Science and Technology (ICTP), Spanish National Research Council (CSIC), Juan de la Cierva 3, 28008, Madrid, Spain

Supporting Information

ABSTRACT: This work is focused on the conductivity study of viscoelastic liquids, taking as a model poly(2,3-dimethoxybenzyl methacrylate). Each isotherm, displaying the conductivity in the frequency domain, shows a plateau in the low frequency region, representing the dc conductivity. The covered frequency range by the plateau increases with the temperature. The frequency corresponding to the end of the plateau, ω_c, marks the onset of the ac conductivity, which correspond in increasing order of frequency to Maxwell−Wagner−Sillars, glass−rubber transition and secondary relaxations. The contributions of the relaxation processes to the ac conductivity in the wholly frequencies range were analyzed. The time−temperature correspondence principle holds for the reduced ac conductivity. However, this principle does not hold for the components of the complex dielectric permittivity due, among other things, to the different temperature dependences of each dipolar relaxation processes. Analogueies and differences between the conductivity behavior of viscoelastic liquids and disordered inorganic solids are discussed.

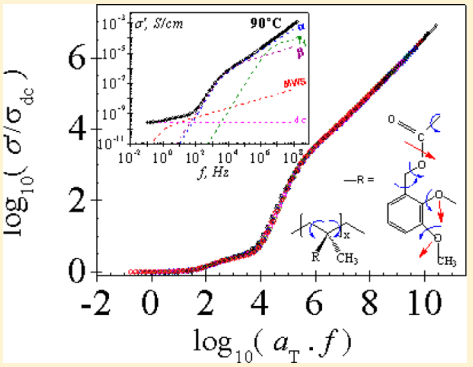

1. INTRODUCTION

In the frequency domain, the response of viscoelastic liquids to alternating mechanical force fields involves, in decreasing order of frequency, the following processes: (a) secondary relaxations associated with local motions in the side chains, the backbone or both, (b) the glass−rubber or α-relaxation arising from segmental motions, and (c) the normal relaxation produced by chains disentanglement that give rise to flow.[1−4] Since the α relaxation freezes at T_g and the low frequency side of this relaxation overlaps with the high frequency side of the normal mode process, the glass−rubber relaxation is considered the precursor of the glassy state and liquid flow.

The experimental devices used in the mechanical measurements may present some limitations at frequencies above 50−100 Hz caused by their own-resonance. This fact precludes the experimental study of the fast secondary relaxations of viscoelastic liquids, consequently, the study of these processes by mechanical methods is mostly restricted to temperatures below T_g. On the other hand, responses associated with slower processes, such as the glass−rubber and the normal mode relaxations, can only be measured at a given temperature, in a time/frequency window of about four-five decades. As a result, the viscoelastic behavior of viscoelastic liquids over long time/frequency windows can only be obtained for thermoviscoelastic simple systems.[5] Nevertheless, master curves covering 12 or more decades in the frequency/time domain, can be obtained for these systems by superposing the isotherms representing viscoelastic functions in the frequency/time domain with the isotherm corresponding to a reference temperature. However, the isotherms superposition requires that the time/frequency temperature correspondence holds, i.e. the relaxation times associated with the different relaxation mechanisms must have the same temperature dependence.[6] This might be so for the α and the normal mode relaxations, which are governed by the thermodynamic variables volume and temperature. On the other hand, creep experiments carried out on monodisperse polystyrene, using Plazek's[7] frictionless creep apparatus, showed that the time-correspondence principle does not hold for the creep compliance function $J(t)$, though it does for the recovery creep compliance $J_r(t) = J(t) - t/\eta$ (where η is the zero-shear rate viscosity). This means that the relaxation times associated with segmental motions and with chains disentanglement do not have the same temperature dependence. On the other hand, since secondary relaxations are thermally activated processes,[8] the time temperature correspondence may not hold in the region where the fast relaxations overlap with

Received: January 31, 2013
Revised: March 12, 2013

   dx.doi.org/10.1021/ma400224x | Macromolecules XXXX, XXX, XXX−XXX

the slower α absorption.[1,9] Strictly speaking, the frequency temperature correspondence might hold in wide frequency/time range for the recovery compliance function only for the systems (i) where the changes in the viscoelastic functions caused by the secondary processes are negligible or (ii) where severe overlapping between the α and the secondary relaxations is absent.

An alternative for the chains motions study in a wide time/frequency window is the dielectric spectroscopy technique, which may cover 12 or more decades at a single temperature.[8,10−13] The ac electrical response of disordered systems to electric perturbation fields is the result of different contributions superposition. These contributions are related to: (i) the hopping process of localized charge carriers, (ii) the dispersive response of the bound charges (dipolar response), and (iii) the response produced by the molecular structure deformation, following the diffusion of charges through percolation paths.[14] The dipolar response presents at high frequencies one or more secondary relaxations. These processes are followed in decreasing order of frequency by the glass−rubber relaxation.[8,15−17]

This paper focuses on the effect of the dipolar relaxations on the time−temperature correspondence for the ac conductivity of polar viscoelastic liquids. Poly(2,3-dimethoxybenzyl methacrylate) (PDMB23) was taken as the model, whose repeat unit is shown in Figure 1. Earlier work carried out on this polymer[18]

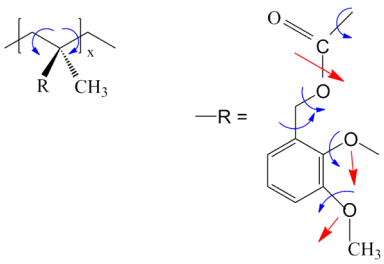

Figure 1. Structure scheme of the PDMB23.

showed that side groups segregation from the backbone promotes relatively long distance charge jumps, reflected as a distributed Maxwell−Wagner−Sillars (MWS) relaxation[19−23] in the low frequency side of the spectra. The aim of this work is to inquire the effects of the MWS process and the strong dispersive processes, arising from the complex motions of polar viscoelastic liquids, on the time−temperature correspondence of the ac conductivity. Attention is also paid to the time−temperature correspondence of the complex dielectric permittivity. It will be shown that the ac conductivity of polar viscoelastic liquids exhibits the main characteristic features displayed by the ac conductivity of disordered solids. However, in the latter case the local and segmental motions characteristic of these systems strongly affect the ac conductivity.

2. EXPERIMENTAL PART

2,3-Dimethoxybenzyl methacrylate was obtained by reaction of 2,3-dimethoxybenzyl alcohol with methaloyl chloride at reflux temperature using toluene as solvent, following the procedure described elsewhere.[24] The monomer was isolated from the reaction medium at reduced pressure (80−95 °C, 1 mmHg pressure). The polymerization of 2,3-dimethoxybenzyl methacrylate was carried out in toluene solution, at 50 °C, under nitrogen atmosphere, using α,α'-azobis(isobutyronitrile) (AIBN) as initiator. The poly(2,3-dimethoxybenzyl methacrylate) was precipitated with methanol dissolved in chloroform, precipitated again with methanol, washed several times with methanol and dried in a vacuum oven at 60 °C. The average molecular weight of PDMB23 measured by GPC was 1.4×10^5 and the heterodispersity index was 1.8. The stereochemical structure of the polymer determined by NMR was atactic. The obtained T_g was 47 °C, measured by DSC and taken as the temperature at the midpoint of the endotherm.

The complex impedance of PDMB23 was measured with a Novocontrol broadband dielectric spectrometer (Hundsagen, Germany), integrated by a SR lock-in amplifier with an Alpha dielectric interface and an Agilent 4991 coaxial line reflectometer, to carry out the measurements in the frequency range 10^{-2}−10^6 Hz and 10^6−10^9 Hz, respectively. The electrodes were gold disks of 20 and 10 mm of diameter for the measurements carried out at low and high frequencies, respectively. The temperature was controlled by a nitrogen jet (QUATRO) from Novocontrol with a temperature error of 0.1 °C during every single sweep in frequency.

3. CONDUCTIVITY FUNDAMENTALS

Under an alternating voltage $V(\omega) = V_0\,\mathrm{Im}[\exp(j\omega t)]$, where ω is the angular frequency of the electric field ($\omega = 2\pi f$), the current crossing a sample sandwiched between two parallel plane electrodes is $i = dq/dt = V(\omega)/Z^*(\omega)$, where q is the charge of the capacitor and $Z^*(\omega)$ is the complex impedance.[12,25] The admittance of the sample is $Y^*(\omega) = 1/Z^*(\omega)$ and taking into account that the conductivity is expressed in terms of the admittance by $\sigma^*(\omega) = Y^*(\omega)A/l$, the dielectric permittivity and the conductivity are found to be related by $\varepsilon^*(\omega) = \sigma^*(\omega)/j\varepsilon_0\omega$. On the other hand, the complex electrical modulus $M^*(\omega) = 1/\varepsilon^*(\omega)$ is an important parameter to separate charges transport from dipolar processes.

The beauty of the linear dielectric analysis is that impedance data allow the estimation of different dielectric functions related to: (a) dipoles motions associated with local and cooperative micro-Brownian motions of the molecular chains and (b) charges transport across the samples. In principle, the equivalent circuit modeling the complex impedance in the frequency domain is made up of a constant phase element of admittance $Y^*(\omega) = Y_0(j\omega)^a$ $(0 < a \leq 1)$ in parallel with a polarization resistance R_p. In these circumstances, the impedance of the equivalent circuit is given by[25]

$$Z^*(\omega) = \frac{R_p}{1 + (j\omega\tau)^a} \tag{1}$$

where $Y_0R_p = \tau^a$, being τ a mean-relaxation time. For some systems, the Cole plots are skewed arcs along a nearly straight line at high frequencies, and $Z^*(\omega)$ is better expressed in terms of the Havriliak−Negami equation[26−29]

$$Z^*(\omega) = \frac{R_p}{[1 + (j\omega\tau)^a]^b} \tag{2}$$

The shape parameters a, b lie in the range $0 < a, b \leq 1$.

4. RESULTS AND DISCUSSION

a. Conductivity and Dipolar Relaxation Processes. Cole−Cole impedance plots, at several temperatures, are deformed arcs roughly described by eq 2, that intersect the abscissa axis at the extreme frequencies in such a way that $Z'(\infty) = 0$ and $Z'(0) = R_p$, being R_p the polarization resistance (Figure 1S Supporting Information). The temperature dependence of the R_p values shows a strong decrease of this parameter with increasing temperature (Figure 2S of the Supporting Information).

dx.doi.org/10.1021/ma400224x | Macromolecules XXXX, XXX, XXX−XXX

Figure 2 shows the double logarithmic plots of the real component σ' of the complex conductivity σ^* in the frequency

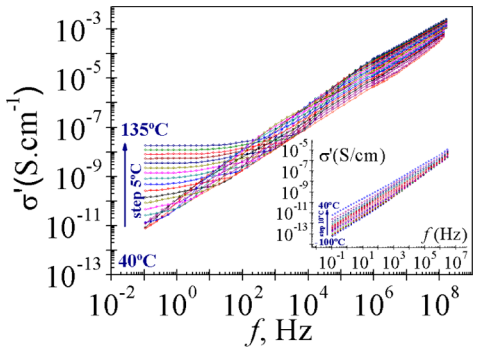

Figure 2. Frequency dependence of the real component σ' of the complex conductivity σ^* at several temperatures (from 40 to 135 °C, step 5 °C, and in the inset from −100 to −40 °C, step 10 °C).

domain at several temperatures. As usual, in the frequency domain, the isotherms corresponding to high temperatures, exhibit a plateau in the low frequency region, reflecting a frequency independent conductivity, i.e., dc conductivity. The covered frequency range by the plateau increases with temperature. Figure 3 shows the dc conductivity values as a

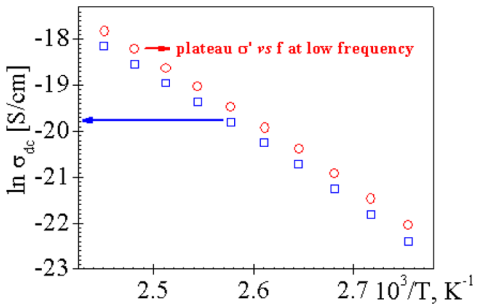

Figure 3. Dc conductivity at different temperatures of interest evaluated from the low frequency plateau and using the relationship $\sigma_{dc} = lA/R$.

function of the reciprocal of the absolute temperature. These values were estimated from: (i) the R_p values by means of the relationship $\sigma_{dc} = l/R_pA$ and (ii) the plateau at low frequencies of the σ' plots. In both cases, the obtained R_p values are in a reasonable good agreement.

Figure 4 shows the values of ω'_c for the isotherms as a function of the reciprocal of temperature. These values were

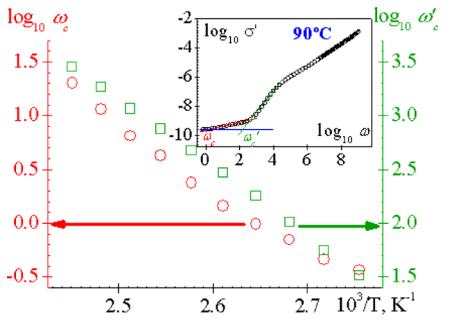

Figure 4. Temperature dependence of the critical frequency ω'_c for PDMB23. Inset shows the graphic determination of ω'_c.

estimated as the frequency at which the dc line intersects with the slope drawn at the inflection point of the isotherm of interest. As we can see in this Figure, a sharp increase in σ' occurs at a frequency ω'_c, located at 150.5 rad·s^{-1}, at 90 °C. At high frequencies, the double logarithmic plot of the conductivity vs frequency converges to a straight line, i.e., the ac conductivity exhibits the power law $\sigma' \sim \omega^n$. It is worth noting that at $T < T_g$ the ac conductivity of PBDM23 nearly obeys the power law in almost the wholly frequencies range (see inset in Figure 2).

A thorough inspection of the σ' isotherms in the frequency domain, corresponding to the viscoelastic liquid, shows that the departure of σ' from dc conductivity actually occurs at a frequency $\omega_c \cong \omega'_c/100$, caused by a process whose nature will be discussed latter. Then, the frequency ω_c can be considered the crossover frequency marking the onset of the ac conductivity. It is worth noting that ω_c like ω'_c shifts to higher values with increasing temperature.

Dipolar dispersive processes, responsible for the abrupt increase of the ac conductivity at $\omega > \omega'_c$, are better reflected by expressing the impedance results in terms of the complex dielectric permittivity ε^*. Isotherms for the real permittivity ε', in the frequency domain, are shown in a relatively wide range of temperatures in Figure 5. As usual, ε' increases with decreasing

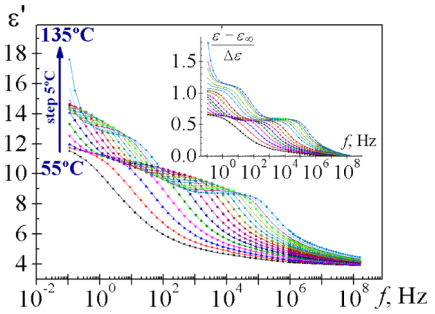

Figure 5. Frequency dependence of the real permittivity ε' in wide range of temperatures corresponding to PDMB23 (55−135 °C, step 5 °C).

frequency reaching a plateau that corresponds to the relaxed dielectric permittivity. However, after the plateau, ε' further increases with decreasing frequency until a second plateau is reached at a frequency that roughly coincides with the frequency ω_c, which marks the onset of the ac conductivity in the σ' isotherms. The interpretation of the X-ray diffractograms of PDMB23 carried out elsewhere[18] suggests the presence of nanodomains in the viscoelastic liquid, formed by polar side groups which are flanked by the backbone. Long distance charge transport across the interfaces of the nanodomains produces a distributed MWS relaxation, reflected in the increase of ε' from the first to the second plateau. The further increase of ε' with decreasing frequency observed in the isotherms at even lower frequencies and high temperatures is attributed to interfacial polymer−electrode phenomena.

MWS process can be attributed to the buildup of charges at the interfaces of the heterogeneous systems. Consequently, it is generally evident in nonhomogenous materials like multiphase polymers,[18,30,31] blends and colloids,[32] crystalline or liquid crystalline polymers,[33] composites,[34,35] etc.. But recently, there is evidence that this process is not unique to multicomponent systems, since their presence has been detected in some complex homopolymers. An example of this kind of complex

dx.doi.org/10.1021/ma400224x | Macromolecules XXXX, XXX, XXX−XXX

homopolymers is the family of poly(*n*-alkyl methacrylates) Structural studies based on X-ray diffraction have shown the aggregation of the side groups of different monomeric units, forming self-assembled alkyl nanodomains, their sizes being related to the length of the side group.

The dielectric loss in the frequency domain is shown at several temperatures in Figure 6. At high frequencies, the loss

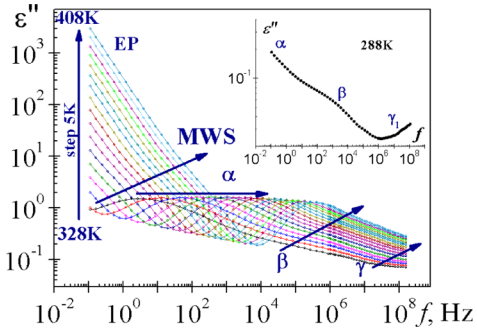

Figure 6. Dielectric loss in the frequency domain at several temperatures for PDMB23 (55−135 °C, step 5 °C). Inset: frequency dependence of the loss permittivity at 15 °C.

isotherms present a relaxation, named γ process, whose low frequency side overlaps with the comparatively stronger secondary β absorption. The low frequency side of the β process overlaps with the high frequency side of the ostensible glass−rubber or α relaxation. In turn, the low frequency side of the α relaxation strongly overlaps with the MWS relaxation. This latter process undergoes a strong overlapping with the contributions to the dielectric loss of the dc conductivity and polymer-electrode interfacial phenomena. In all cases, the overlapping degree between neighboring relaxations increases with temperature.

In order to study how the dipolar activity and the MWS process affects σ', the complex dielectric permittivity was expressed in terms of Havriliak−Negami type equations,[26−29] describing the relaxations processes involved in the response of the system to the perturbation field. The pertinent expression is given by

$$\varepsilon^*(\omega) = \sum_i \frac{(\varepsilon_{ri} - \varepsilon_{\infty})_i}{[1 + (j\omega\tau_i)^{a_i}]^{b_i}} + \frac{\sigma_{dc}}{j\varepsilon_o\omega} \quad (3)$$

where σ_{dc} and ε_0 represent, respectively, the dc conductivity and the permittivity of the empty space. The subscript i refers to the relaxation processes involving the secondary absorptions, the glass−rubber and MWS relaxations, i.e., $i = \gamma, \beta, \alpha$, MWS. The subscripts r and ∞ in eq 3 indicate, respectively, relaxed and unrelaxed dielectric permittivities, so that $\Delta\varepsilon_i = \varepsilon_{ri} - \varepsilon_{\infty i}$ represents the dielectric strength of the relaxation i. The shape parameters a and b determine the departure of the relaxations from Debye behavior. For secondary relaxations and MWS process the value of b is the unit, but this parameter lies in the range $0 < b \leq 1$ for the α relaxation. Using minimization methods, the parameters that describe eq 3 were computed from the dielectric loss and the pertinent results for a_γ, a_β, $a_\alpha a_{MWS}$, b_α, $\Delta\varepsilon_\gamma$, $\Delta\varepsilon_\beta$, $\Delta\varepsilon_\alpha$, $\Delta\varepsilon_{MWS}$ and σ_{dc} are collected in Table 1.

Let us consider now the changes in σ' caused by the dipolar relaxations and by the MWS process, taken as an example the isotherm at 90 °C in Figure 2. For this purpose, in Figure 7 are

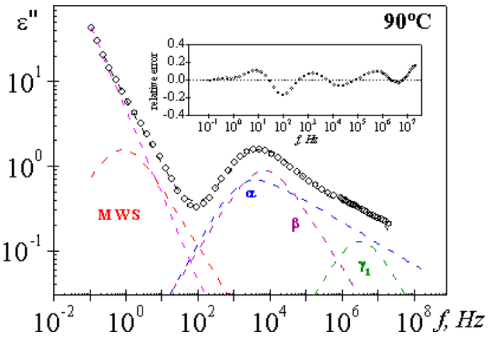

Figure 7. Dielectric loss permittivity for PDMB23 in the frequency domain at 90 °C.

Table 1. HN Fit Parameters for $\varepsilon''(\omega)$ at Several Temperatures for PDMB23

T (°C)	$\Delta\varepsilon_\alpha$	$\Delta\varepsilon_{\alpha'}$	$\Delta\varepsilon_\beta$	$\Delta\varepsilon_{\gamma1}$	a_α	$a_{\alpha'}$	a_β	$a_{\gamma1}$	b_α	$b_{\alpha'}$	$\log_{10}\tau_\alpha$ [s]	$\log_{10}\tau_{\alpha'}$ [s]	$\log_{10}\tau_\beta$ [s]	$\log_{10}\tau_{\gamma1}$ [s]
55	6.02			0.12	0.55			0.68	0.40		−0.38			−5.80
60	4.75		2.36	0.12	0.72		0.58	0.48	0.33		−1.15		−2.93	−6.15
65	4.38		2.53	0.13	0.74		0.61	0.54	0.34		−1.83		−3.23	−6.33
70	3.99		2.71	0.14	0.76		0.62	0.61	0.34		−2.36		−3.57	−6.46
75	3.86		2.84	0.15	0.78		0.64	0.66	0.35		−2.83		−3.86	−6.69
80	3.85		2.99	0.16	0.80		0.66	0.70	0.37		−3.27		−4.14	−6.85
85	3.78	4.27	3.14	0.17	0.80	0.65	0.66	0.73	0.38	1.00	−3.71	−0.38	−4.39	−7.08
90	3.77	3.87	3.24	0.18	0.81	0.69	0.67	0.74	0.39	1.00	−4.17	−0.71	−4.64	−7.30
95	5.69	3.75		0.20	0.69	0.70		0.75	0.55	0.99	−4.53	−0.97		−7.53
100	5.49	3.72		0.20	0.70	0.71		0.72	0.55	0.99	−4.91	−1.19		−7.76
105	5.30	3.69		0.21	0.70	0.69		0.69	0.55	1.00	−5.17	−1.46		−7.95
110	5.08	3.45		0.21	0.70	0.70		0.67	0.55	1.00	−5.41	−1.72		−8.10
115	4.90	3.34		0.21	0.71	0.72		0.66	0.55	1.00	−5.61	−1.92		−8.20
120	4.72	3.34		0.22	0.71	0.72		0.66	0.55	1.00	−5.83	−2.10		−8.38
125	4.55	3.16		0.23	0.71	0.73		0.66	0.56	1.00	−6.00	−2.30		−8.50
130	4.40	3.13		0.23	0.71	0.73		0.66	0.58	1.00	−6.19	−2.46		−8.65
135	4.27	3.09		0.24	0.71	0.73		0.67	0.60	1.00	−6.36	−2.61		−8.77
uncertainty	±0.01	±0.01	±0.01	±0.01	±0.01	±0.01	±0.02	±0.02	±0.02	±0.01	±0.02	±0.02	±0.02	±0.02

dx.doi.org/10.1021/ma400224x | *Macromolecules* XXXX, XXX, XXX−XXX

plotted the contributions of the individual relaxations to the loss isotherm calculated from the parameters that describe the different dielectric relaxations collected in Table 1. The errors involved in the calculation, i.e. $(\varepsilon''_{calc} - \varepsilon''_{exptl})/\varepsilon''_{exptl}$, are represented in the inset of the figure. Taking into account that $\sigma'(\omega) = \omega\varepsilon_0\varepsilon''(\omega)$, the changes in the ac conductivity by effect of the dipolar relaxations and the MWS process were calculated and the pertinent contributions are shown in Figure 8. The ac

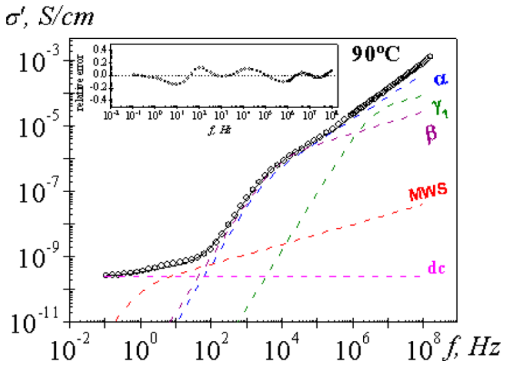

Figure 8. Dielectric conductivity for PDMB23 in the frequency domain at 90 °C. The pink line represents the dc conductivity, the red line the MWS process, the blue line the α-relaxation, the purple the β-relaxation, and the green line the γ-relaxation. The black line represents the dielectric loss permittivity recalculated from the deconvoluted relaxations. Inset: relative error calculated as $(\sigma'_{calcd} - \sigma'_{exptl})/\sigma'_{exptl}$.

conductivity calculated from the sum of the contributions of the relaxations is indicated by a continuous line in the σ' isotherm, while the relative errors involved in the calculation of σ', i.e., $(\sigma'_{calc} - \sigma'_{exptl})/\sigma'_{exptl}$, are shown in the inset of Figure 8. Taking into account that in the high frequency range $(\omega \rightarrow \infty)$, the dielectric loss of the secondary and MWS relaxations scales as $\varepsilon'' \sim \omega^{-a}$ whereas the glass−rubber or α relaxation scales as $\varepsilon'' \sim \omega^{-ab}$, the following scaling laws are obtained

$$\sigma_i'(\omega) \sim \omega^{1-a}; \quad i = \gamma, \beta, \text{MWS} \tag{4}$$

$$\sigma_\alpha'(\omega) \sim \omega^{1-ab} \tag{5}$$

The red line represents the α-relaxation, the blue line the β-process, and the green line the γ-relaxation. The black line represents the dielectric loss permittivity recalculated from the deconvoluted relaxations. Inset: relative error calculated as $(\varepsilon''_{calcd} - \varepsilon''_{exptl})/\varepsilon''_{exptl}$.

The double−logarithmic plot of the contribution of each secondary relaxation, as well as the MWS process, to the ac conductivity is a straight line with slope $1 - a$, in the high frequency limit. Accordingly, the lower the exponent a (or the higher the departure from a Debye process), the larger the slope of the straight line is. For the α relaxation, the product of the shape factors, ab, governs the terminal ac conductivity in such a way that, the lower the product ab, the higher the slope of the contribution of the α relaxation in the limit $\omega \rightarrow \infty$ is. The upper bound limit of the slope is 1 that corresponds to $a = b = 0$. Notice that for a Debye relaxation $a = b = 1$, and $\lim_{\omega\rightarrow\infty}[d[\log \sigma'(\omega)]]/d[\log \omega] = 0$, i.e. the ac conductivity is independent of frequency. Then, $0 < \lim_{\omega\rightarrow\infty}[d[\log \sigma'(\omega)]]/d[\log \omega] \leq 1$ for the contributions of the individual relaxations to σ' at $\omega \rightarrow \infty$.

b. Time Temperature Correspondence. The σ' isotherms were normalized with respect to the dc conductivity (see Figure 9) and shifted to the reference isotherm (135 °C).

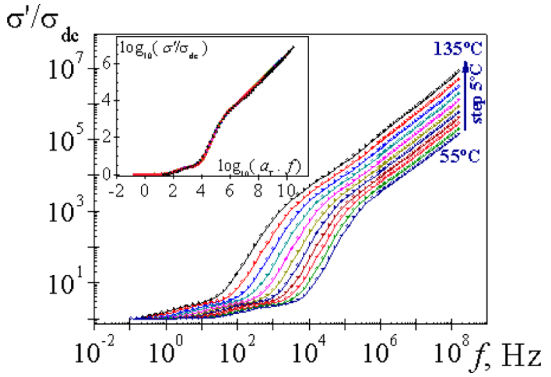

Figure 9. σ' isotherms normalized with respect to the dc conductivity. The inset shows the master curve obtained using as the reference isotherm T_0 = 135 °C.

The isotherms superpose rather well over the isotherm of reference, obtaining the master curve shown in the inset of Figure 9. Notice that the master curve extends over roughly 12 decades. The frequency−temperature correspondence principle holds and the empirical shift factors a_T used are plotted as a function of temperature in Figure 10. An inspection of Figure 4

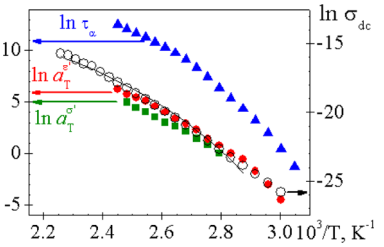

Figure 10. Temperature dependence of the empirical shift factors a_T (left-full square, σ', and left-full circle, ε'), τ_α (left-full triangle), and σ_{dc} (right-open circle).

inset clearly reveals the frequency ω_c at which the ac conductivity experiences a slow increase reaching a small plateau, followed by a sharp increase of σ' with increasing frequency at a frequency ω'_c. The double logarithmic plot of σ' vs ω at high frequencies is a straight line of slope 0.75. It is worth noting that the extrapolation of the straight line to the low frequency region intercepts the σ' isotherm at ω_σ, the frequency at which the low frequency side of the MWS relaxation intercepts with the abscissa axis.

A general approach for the study of the time/frequency temperature correspondence for the ac conductivity is to use the scaling ansatz[36−38]

$$\sigma'(\omega, T) = \sigma_{dc} f[\omega/\omega_c(T)] \tag{6}$$

where $f(\omega/\omega_c)$ is the so-called scaling function and ω_c the previously defined angular frequency marking the onset of the ac conductivity. The results show that the scaling law not only holds for disordered ion conducting inorganic systems, but also for polar viscoelastic liquids (see Figure 3S of Supporting Information). Long ago, several authors[39−41] formulated an empirical expression that permits to estimate ω_c in terms of the dc conductivity σ_{dc} and of the dielectric strength $\Delta\varepsilon$ in

dx.doi.org/10.1021/ma400224x | Macromolecules XXXX, XXX, XXX−XXX

disordered inorganic ion conducting systems. This expression is known as the BNN equation and is given by

$$\omega_c = \frac{\sigma_{dc}}{p\varepsilon_0 \Delta\varepsilon} \tag{7}$$

where p is a parameter of the order of unity. Dyre et al.[14] have shown that through the low-frequency expansion of the conductivity, a connection between eqs 6 and 7 can be made. Actually, according to eq 6, the complex conductivity at $\omega \to 0$ can be written as $\sigma^*(\omega) = \sigma_{dc}(1 + jK\omega/\omega_c)$ where K is a real parameter. So dividing the two sides of this expression by $j\varepsilon_0\omega$, taking into account that $\varepsilon^*(\omega) - \varepsilon_\infty = \sigma_{ac}^*(\omega)/j\varepsilon_0\omega$, and equating the real components, in the limit $\omega \to 0$, it is obtained that $\varepsilon(0) - \varepsilon_\infty = \Delta\varepsilon = K\sigma_{dc}/\omega_c$. Notice that $K = 1/p\varepsilon_0$. The values of ω_c calculated by means of eq 7, using $p = 1$, are compared in Figure 11 with those estimated from the isotherms. It can be seen that the calculated values lie roughly one decade below than those estimated from the BNN equation. However, the results corresponding to ω'_c (the frequency that marks the onset of the glass–rubber relaxation, Figure 4), are in satisfactory agreement with those predicted by eq 7. This means, according to our results, that the BNN equation only holds for polar viscoelastic liquids where MWS process is absent.

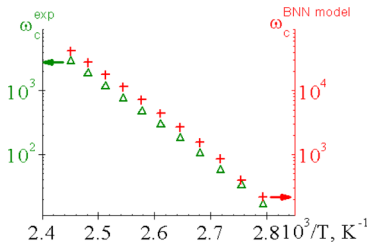

Figure 11. Temperature dependence of ω_c(Hz) obtained from the experimental isotherm (triangle-left) and from BNN model (plus-right).

c. Time–Temperature Correspondence for Dipolar Processes. Figure 12 shows the master curve obtained by shifting the isotherms representing values of $(\varepsilon' - \varepsilon_\infty)/\Delta\varepsilon$ over the 80 °C reference isotherm. It can be seen that the superposition is rather poor, in spite of the fact that a vertical shift to improve the superposition was employed. The failure is even more visible if the reduced isotherms for ε' are expressed in the logarithmic form (inset Figure 12). As can be seen in Figure 12, a good superposition is obtained at low frequencies but a great dispersion is observed at high frequencies, where dipole mechanisms that give rise to the glass–rubber and the secondary relaxations are active. The cause of the failure is multiple. For example, an increase in temperature hinders the alignment of the dipoles with the electric field in the glass–rubber relaxation, thus reducing the relaxed dielectric permittivity and decreasing the height of the plateau. As a result, the width of the glass rubber relaxation tends to decrease with increasing temperature as show the PBDM23 data reported[18] for the stretch exponent of the KWW equation. The vertical shifts necessary to superpose the plateaus, may not superpose the secondary relaxations. On the other hand, an augment of temperature tends to increase the dielectric strength of secondary relaxations. In order to the time–temperature correspondence holds, an important condition is that the relaxation times of all relaxations have similar temperature dependence. However, that dependence is much stronger in the glass–rubber relaxation than in the secondary processes. Therefore, the time–temperature correspondence for the components of the complex dielectric permittivity might only hold for weakly polar polymer systems. In this regard, Zorn et al. found a good time–temperature superposition for the dielectric loss of polybutadienes. The superposition only failed in the samples of polybutadiene with the lowest fraction of vinyl content (0.07).[42] In spite of the reasons indicated above for the failure of the time–temperature superposition of the dielectric permittivity in polar polymers, Zhao and McKenna[43] recently reported a good time–temperature superposition for poly(vinyl acetate) at $T > T_g$. However, a detailed analysis of the secondary relaxations, especially dielectric strengths and temperature dependence, has not been discussed.

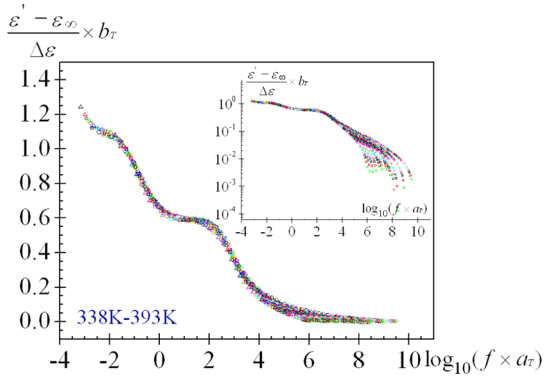

Figure 12. Master curve of the dielectric permittivity normalized for PDMB23 in the frequency domain (T_0 = 80 °C).

d. Temperature Dependence of the Conductivity and Relaxation Processes. As usual, the PBDM23 secondary relaxations, γ and β, obey Arrhenius behavior with activation energies in kJ mol^{-1} of 95 and 132, respectively. The faster absorption, the γ process, is attributed to motions of the terminal dimethoxy phenyl group, whereas the β relaxation is associated with motions of the side groups, which are alone or coupled with local motions of the backbone. The relative closeness of the activation energies for the two relaxations suggests that the β process is presumably only produced by motions restricted to the side groups.

Figure 10 shows the Arrhenius plots for σ_{dc} and a_T (used in the generation of the dielectric permittivity and conductivity master curves), which remind the temperature dependence of the relaxation time associated with the dipolar glass–rubber relaxation, also shown in the figure. This means that the ac charge transport is governed by both, the free volume and the temperature. By assuming that the Doolittle equation[44,45] holds, i.e., $\sigma(\omega,T) \sim [B/\Phi(T)]$, where Φ is the relative free volume and B is a parameter close to the unit, the Vogel–Fulcher–Tamman–Hesse (VFTH) equation[46,48] is obtained. Actually, since the specific volume v is related to temperature by $v = v_0 + \alpha_f(T - T_V)$, where T_V is the Vogel temperature[46] (or the temperature at which the configurational entropy of the system is nil) and α_f is the expansion coefficient ($\alpha_f = (1/v)(\partial v/\partial T)_P$), σ is given by

$$\sigma(\omega, T) = A \exp\left(\frac{m}{T - T_V}\right) \tag{8}$$

dx.doi.org/10.1021/ma400224x | Macromolecules XXXX, XXX, XXX–XXX

where $m = Bv_0/\alpha_f$, being v_0 the occupied volume in the specific volume v. The inset of Figure 4 shows that σ' is described by eq 2. Combining the Doolittle equation[44,45] with eq 8 yields $\Phi_g/B = (T_g - T_v)/m$, where Φ_g is the relative free volume at T_g. Taking into account that $T_V = 265$ K, and assuming that $B = 1$, we obtained $\Phi_g = 4.0 \times 10^{-2}$ and $\alpha_f = 7.3 \times 10^{-4}$ K^{-1}. These last parameters, obtained from the Arrhenius fit ($\ln \tau_\alpha$ vs T^{-1}), are 3.4×10^{-2} and 6.2×10^{-4} K^{-1}, respectively.[18]

e. Conductivity Mechanisms and Concentration of Ionic Species. The conductivity mechanism in solid disordered systems is explained by the random barrier model (RBM).[49] The model considers the hopping of a simple particle on a lattice, with barrier energies between neighboring sites randomly drawn from a smooth probability distribution. The obtained results, for the evolution of the ac conductivity of viscoelastic liquids, can also be interpreted in terms of this model. Thus, the rather sharp decrease of the ac conductivity, in the frequency region where dispersive processes occur, is a consequence of the fact that local relaxations together with the glass−rubber relaxation contribute to the topological disorder of the material. As a result, the energy barriers of the charge transport undergo an anomalous increase, hindering the back and forth motion of the charges that contribute to the dispersive ac conductivity. The departure of the ac conductivity from the power law is comparatively small for viscoelastic liquids in the glassy state, where only secondary relaxations are displayed.[50] Long range motions that produce dc conductivity need to overcome a percolation barrier energy E_c, in such a way that the time necessary to accomplish it is $t_c \sim \exp(-E_c/k_BT)$.[51] The reciprocal of t_c marks the onset of the dc conduction,[49] i.e., $\omega_c \cong t_c^{-1}$. E_c acting as a bottleneck explains the Arrhenius behavior of the dc conductivity. However, it is worth noting that the plot of ω_c vs the reciprocal of temperature is not a straight line.

Schröder and Dyre have recently shown[52] that if $\bar{\sigma} = \sigma^*(\omega)/\sigma_d$ and $\bar{\omega}$ is a suitable scaled frequency, i.e., ω/ω_c, the RBM theory predicts at $\omega > \omega_c$ that

$$\ln \bar{\sigma} = \left(\frac{j\bar{\omega}}{\bar{\sigma}}\right)^{2/3} \tag{9}$$

A better expression in the whole frequency range is[52]

$$\ln \bar{\sigma} = \frac{j\bar{\omega}}{\bar{\sigma}}\left(1 + \frac{8}{3}\frac{j\bar{\omega}}{\bar{\sigma}}\right)^{-1/3} \tag{10}$$

As shown in Figures 4S and 5S of the Supporting Information, neither eq 9 nor eq 10 fit to the ac conductivity in the frequency domain. However, the fitting should be significantly better for PBDM23 in the glassy state, where segmental motions are frozen. Unfortunately, the fact that the dc conductivity of polar polymers in the glassy state cannot be estimated impedes the testing of these expressions in glassy PBDM23.

e.1. Concentration of Residual Ionic Species. In principle, the concentration of residual ionic species in viscoelastic liquids that produce dc conductivity can be estimated using phenomenological Nernst type equations to describe ion motion in these systems. However, unlike disordered ion conducting materials, which contain specific ions responsible for the dc conductivity in the glassy state and in the melt, the chemical nature of the transport charges in viscoelastic liquids is unknown. The dc conductivity observed in polymers, except in electronic and ionic conducting polymers, proceeds from humidity traces, impurities present in the reactants, solvents, etc. used in the synthesis of the material. In order to estimate the concentration of ion impurities in viscoelastic liquids, it would be necessary to know beforehand the diffusion coefficients of the ions by other methods, as pulsed field gradient RMN, and to assume the value of 1 for the Haven ratio. Nevertheless, since the nature of the ions is unknown, their concentration cannot be obtained from RMN results and dielectric conductivities. Models have been described based on the motion at low frequencies of the macrodipole, produced by the charges accumulation at the polymer-electrode interface at very low frequencies, which allows the determination of charge impurities.[53−57] However, the concentration of ions estimated by the models has not been experimentally tested and the reliability of the results predicted is unknown. The polarization phenomena can be quantitatively reproduced by an approach and the observed scaling laws at the interface between the electrode and the ion conductor has recently been formulated. Nevertheless, the approach does not address the estimation of the concentration of ionic species.[58]

e.2). Ac Conductivity at High Frequencies. For a variety of solids including glassy, crystalline and molten ion conductors, independent of the physical and chemical structures, the ac conductivity in the high frequency region follows the power law $\sigma'(\omega) = A\omega^n$, with $n \cong 1$.[59,60] This zone is called the nearly constant loss (NLC) regime, because it corresponds to the frequency region in which the dielectric permittivity is nearly independent of frequency. The isotherms representing the PBDM23 ac conductivity, shown in Figure 2, also follow the power law at high frequencies. However, the exponent n depends on temperature in such a way that its value lies in the vicinity of 0.75 at $T < 84$ °C, but at $T > 84$ °C, an increase is observed as T decreases reaching a value of about 0.82 at 45 °C (see Figure 13). This behavior suggests that the less relaxed are

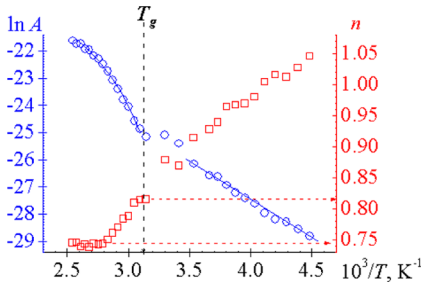

Figure 13. Temperature dependence of the A (circle) and n (square) parameters of the ac conductivity in the high frequency region ($\sigma'(\omega) = A\omega^n$).

the dipoles in the viscoelastic liquid, the higher the exponent is. In the glassy state, the exponent n lies in the vicinity of the unit reaching the value of 1.05 at −50 °C, 97 °C below T_g. On the other hand, whereas the temperature dependence of dc conductivity is of Arrhenius type, so that it is a thermally activated process, the parameter A for PBDM23 only follows Arrhenius behavior at temperatures below T_g (see Figure 13). However, for temperatures above T_g, the dependence of A on the reciprocal of temperature presents a curvature that resembles the behavior of $\sigma'(\omega)$, ω_c, and ω'_c, i.e., the variation of A with T is governed by the free volume and temperature. Therefore, the variation of A with temperature is described by the VFTH equation. Thus, the plot $\ln A$ vs $1/(T - T_V)$ is a straight line whose slope is lower than one-third of that

dx.doi.org/10.1021/ma400224x | Macromolecules XXXX, XXX, XXX−XXX

corresponding to $\sigma'(\omega)$, ω_σ and ω'_c. The possible origin of the NCL regime is discussed in detail elsewhere, Dyre et al.[14] The most recent interpretation suggests that the NCL is the simple extension of the dispersive conductivity to higher frequencies.

5. CONCLUSIONS

The isotherms representing the ac conductivity of viscoelastic liquids in the frequency domain exhibit the same pattern as those corresponding to ion-conducting disordered solids. That is, they present a plateau in the low frequency region corresponding to the dc conductivity until a frequency ω_c is reached, which marks the onset of the ac conductivity. However, owing to strong dipolar relaxation processes taking place in viscoelastic liquids, the increase of the ac conductivity with frequency (at $\omega > \omega_c$) is not so smooth as in the case of ion-conducting disordered solids.

The time−temperature correspondence principle for the ac conductivity of viscoelastic liquids obeys to the scaling ansatz, which governs the time−temperature superposition of ion conducting disordered solids. However, the time-correspondence principle does not hold for the components of the dielectric permittivity of viscoelastic liquids. The frequency at the onset of the ac conductivity, predicted by the BNN equation for the viscoelastic liquid used in this work, is nearly ten times higher than that estimated from the experimental results. However, it coincides with the maximum frequency, ω'_σ at which the dipoles are completely relaxed. The exponent of the power law in the NLC regime approaches to the unit as the temperature of the viscoelastic liquid comes close to T_g. On the other hand, the temperature dependence of proportional constant of the power law A (of the power law constant, A) obeys the VFTH equation at $T > T_g$ and the Arrhenius equation at $T < T_g$.

■ ASSOCIATED CONTENT

Ⓢ Supporting Information

Figure 1S, Cole−Cole impedance plots, at several temperatures for PDMB23; Figure 2S, temperature dependence of the polarization resistance values (R_p); Figure 3S, temperature dependence scaling spectra for the ac conductivity using the scaling ansatz $\sigma'(\omega,T) = \sigma_{dc} f[\omega/\omega_c(T)]$; Figure 4S, blue points representing the experimental data and red points representing the testing with eq 9; and Figure 5S, blue points representing the experimental data and red points representing the testing with eq 10. This material is available free of charge via the Internet at http://pubs.acs.org.

■ AUTHOR INFORMATION

Corresponding Author

*(M.J.S) Telephone: 0034963879327. E-mail: jsanchis@ter.upv.es.

Notes

The authors declare no competing financial interest.

■ ACKNOWLEDGMENTS

This work was financially supported by the DGCYT and CAM through the Grant MAT2012-33483. This work is dedicated in memoriam of Professor Emeritus Evaristo Riande in recognition of his contribution to polymer science.

■ REFERENCES

(1) Ferry, J. D., *Viscoelastic Properties of Polymers*, 2rd ed; John Wiley&Sons: New York, 1980.
(2) Graessley, W. W. *Adv. Polym. Sci* **1974**, *16*, 1−179.
(3) Graessley, W. W. *Adv. Polym. Sci* **1982**, *47*, 67−117.
(4) Riande, E.; Diaz-Calleja, R.; Prolongo, M.; Masegosa, R.; Salom, C. *Polymers Viscoealsticity: Stress and Strain in Practice*; Marcel Dekker: New York, 2000.
(5) Reference 1, chapter 15.
(6) Plazek, D. J. *J. Rheol.* **1996**, *40*, 987.
(7) Plazek, D. J. *J. Phys. Chem.* **1965**, *69*, 3480.
(8) McCrum, N. G.; Read, B. E.; Williams, G. *Anelastic and Dielectric Effects in Polymeric Solids*; Wiley: London, 1967.
(9) Child, W. C., Jr.; Ferry, J. D. *J. Colloid Sci.* **1957**, *12*, 327.
(10) Craig, D. Q.M., *Dielectric Analysis of Pharmaceutical Systems*; Taylor&Francis: London, 1995.
(11) Kremer, F.; Schönhals, A. *In Broadband Dielectric Spectroscopy*; Springer: Berlin, 2003.
(12) Riande, E.; Díaz-Calleja, R., *Electrical Properties of Polymers*; Dekker: New York, 2004.
(13) Floudas, G.; Paluch, M.; Grzybowski, A.; Ngai, K. L. *Molecular Dynamics of Glass-Forming Systems. Effects of Pressure*: Springer−Verlag: Berlin and Heidelberg, Germany, 2011.
(14) Dyre, J. C.; Maass, P.; Roling, B.; Sidebottom, D. L. *Rep. Prog. Phys.* **2009**, *72*, 46501.
(15) Williams, G., *Dielectric Relaxation Spectroscopy of Amorphous Polymer Systems in Keynote Lectures in Polymer Science*; Riande, E., Ed.; CSIC: Madrid, 1995.
(16) Heijboer, J. Ph.D. Thesis, University of Leiden: Leiden, The Netherlands, 1972.
(17) Boyd, R. H.; Smith, G. D. *Polymer Dynamics and relaxations*: Cambridge University Press: Cambridge, U.K., 2007.
(18) Sanchis, M. J.; Carsí, M.; Ortiz-Serna, P.; Domínguez-Espinosa, G.; Díaz-Calleja, R.; Riande, E.; Alegría, L.; Gargallo, L.; Radic, D. *Macromolecules* **2010**, *43*, 5723.
(19) Maxwell, J. C. *Electricity and Magnetism*; Clarendon: Oxford, U.K., 1893.
(20) Wagner, K. W. *Arch. Elektrotech. (Berlin)* **1914**, *2*, 371.
(21) Sillars, R. W. *Inst. Electr. Eng.* **1937**, *80*, 378.
(22) Mijovic, J.; Fitz, B. D.*Novocontrol Application Note Dielectrics 2*; Novocontrol GmbH: Hundsangen, Germany,1998
(23) Perrier, G.; Bergeret, A. *J. Polym. Sci: Part B: Polym Phys.* **1997**, *35*, 1349.
(24) Burtle, G. J.; Turek, W. N. *J. Org. Chem.* **1954**, *19*, 1567.
(25) Barsoukov, E.; Macdonals, J. R., *Impedance Spectroscopy. Theory, Experiment, and Applications*: Wiley Interscience: New York, 2005.
(26) Havriliak, S.; Havriliak, S. J. *Dielectric and Mechanical Relaxation in Materials*; Hanser: Munich, Germany, 1997; p 57.
(27) Havriliak, S.; Negami, S. *J. Polym. Sci., Polym. Symp.* **1966**, *14*, 99.
(28) Havriliak, S.; Negami, S. *Polymer* **1967**, *8* (4), 161.
(29) Ross Macdonald, J. Impedance Spectroscopy. *Ann. Biomed. Eng.* **1992**, *20*, 289−305.
(30) Carsi, M.; Sanchis, M. J.; Diaz-Calleja, R.; Riande, E.; Nugent, M. J. D. *Macromolecules* **2012**, *45*, 3571−3580.
(31) Castagna, A. L.; Fragiadakis, D.; Lee, H.; Choi, T.; Runt, J. *Macromolecules* **2011**, *44*, 7831−7836.
(32) Fragiadakis, D.; Runt, J. *Macromolecules* **2010**, *43*, 1028−1034.
(33) Arous, M.; Ben Arnor, I.; Kallel, A.; Fakhfakh, Z.; Perrier, G. *J.;Phys. Chem. Solids* **2007**, *68*, 1405.
(34) Otegui, J.; Schwartz, G. A.; Cerveny, S.; Colmenero, J. *Macromolecules* **2013**, DOI: dx.doi.org/10.1021/ma302408z.
(35) Hernández, M.; Carretero-González, J.; Verdejo, R.; Ezquerra, T. A.; López-Manchado, M. A. *Macromolecules* **2010**, *43*, 643−651.
(36) Bowen, C. R.; Almond, D. P. *Mater. Sci. Technol.* **2006**, *22*, 719.
(37) Murugaraj, R. *J. Mater. Sci.* **2007**, *42*, 10065.
(38) Papathanassiou, A. N.; Sakellis, I.; Grammatikakis, J. *Appl. Phys. Lett.* **2007**, *91*, 122911.
(39) Barton, J. L. *Verres Refr.* **1966**, *20*, 328.

(40) Nakajima, T. *Annual Report Conference on Electric and Dielectric Phenomena*; National Academy of Science: Washington, DC, 1972; p 168.
(41) Namikawa, H. *J. Non-Cryst. Solids* **1975**, *18*, 783.
(42) Zorn, R.; Mopsik, F. I.; McKenna, G. B.; Willner, L.; Richter. *J. Chem. Phys.* **1997**, *107*, 3645.
(43) Zhao, J.; McKenna, G. B. *J. Chem. Phys.* **2012**, *136*, 154901.
(44) Doolittle, A. K. *J. Appl. Phys.* **1951**, *22*, 1471.
(45) Doolittle, A. K. *J. Appl. Phys.* **1952**, *23*, 236.
(46) Vogel, H. Z. *Phys.* **1921**, *22*, 645.
(47) Fulcher, G. S. *J. Am. Ceram. Soc.* **1925**, *8*, 339.
(48) Tammann, G.; Hesse, W. *Z. Anorg. Allg. Chem.* **1926**, *156*, 245.
(49) Dyre, J. C.; Schrøder, T. B. *Rev. Mod. Phys.* **2000**, *72*, 873.
(50) Obrzut, J.; Page, K. A. *Phys. Rev. B* **2009**, *80*, 195211.
(51) Bunde, A.; Havlin, S. *Fractals and Disordered Systems*; Springer: Berlin,;1996.
(52) Schröder, T. B.; Dyre, J. C. *Phys. Rev. Lett.* **2008**, *101*, 025901.
(53) Coelho, R. *J. Non-Cryst. Solids* **1991**, *131*−*133*, 1136.
(54) Satti, G.; McLachlan, D. S. *J. Mater. Sci.* **2007**, *42*, 6477.
(55) Klein, R. J.; Zhang, S. H.; Dou, S.; Jones, B. H.; Colby, R. H.; Runt, J. *J. Chem. Phys.* **2006**, *124*, 144903.
(56) Compañ, V.; Sorensen, T. S.; Díaz-Calleja, R.; Riande, E. *J. Appl. Phys.* **1996**, *79*, 403.
(57) Sanchis, M. J.; Ortiz-Serna, P.; Carsí, M.; Díaz-Calleja, R.; Riande, E.; Gargallo, L.; Radic, D. *J. Phys. Chem. B* **2011**, *115*, 5730.
(58) Serghei, A.; Tress, M.; Sangoro, J. R.; Kremer, F. *Phys. Rev. B.* **2009**, *80*, 184301.
(59) Burns, A.; Chryssikos, G D.; Tombari, E.; Cole, R. H.; Risen, W. M. *Phys. Chem. Glasses* **1989**, *30*, 264.
(60) Ngai, K. L. *J. Chem. Phys.* **1999**, *110*, 10576.